

Interpretations of the Omega-K Algorithm and Comparisons with other Algorithms

I. G. Cumming, *Member IEEE*, Y. L. Neo, and F. H. Wong

Dept. of Electrical and Computer Engineering

The University of British Columbia, Vancouver, BC, Canada V6T 1Z4.

tel: 604-822-4623 fax: 604-822-5949 ianc@ece.ubc.ca nyewlam@dso.org.sg fhw@mda.ca

ABSTRACT¹ — This paper presents a Fourier interpretation of the Omega-k SAR processing algorithm that helps explain the key Stolt mapping operation. An approximate form of the algorithm is sometimes used, and we explain how both forms of the ω KA compare with the range Doppler and the chirp scaling algorithms. Finally, a brief discussion is given on which radar parameters allow the accurate use of each algorithm.

Key words: SAR processing, Omega-k, Stolt mapping, chirp scaling, range Doppler.

1 Introduction

The Omega-K (ω KA), range Doppler (RDA) and chirp scaling algorithms (CSA) are the three most common precision SAR processing algorithms used for satellite remote sensing data. In order for these algorithms to be implemented efficiently, they use different approximations. The RDA and CSA discard some of the higher order phase terms in their processing, with the result that the range-azimuth coupling is not accurately compensated when the aperture is wide or the squint angle is large.

The ω KA handles the range dependence of the range-azimuth coupling correctly, which gives it the ability to process data acquired over wide azimuth apertures or high squint angles. This is because the data are processed entirely in the two-dimensional frequency domain, where the approximations used in the CSA and RDA are not needed. However, the ω KA does make another approximation, which hinders its ability to handle large range swaths rather than its ability to handle wide apertures.

In this paper, a overview of ω KA is presented, concentrating on its unique interpolation step, referred to as Stolt mapping. In this one operation, the residual Range Cell Migration Correction (RCMC), secondary range compression (SRC) and azimuth compression are done simultaneously. New Fourier interpretations of the Stolt mapping are given, which help explain the components of the mapping.

¹ This work is supported by the MacDonald Dettwiler/NSERC Industrial Research Chair in Radar Remote Sensing.

2 Overview of the ω KA

Block diagrams of accurate and approximate implementations of the ω KA algorithm are given in Figure 1.

(a) Accurate WKA algorithm

(b) Approximate WKA algorithm

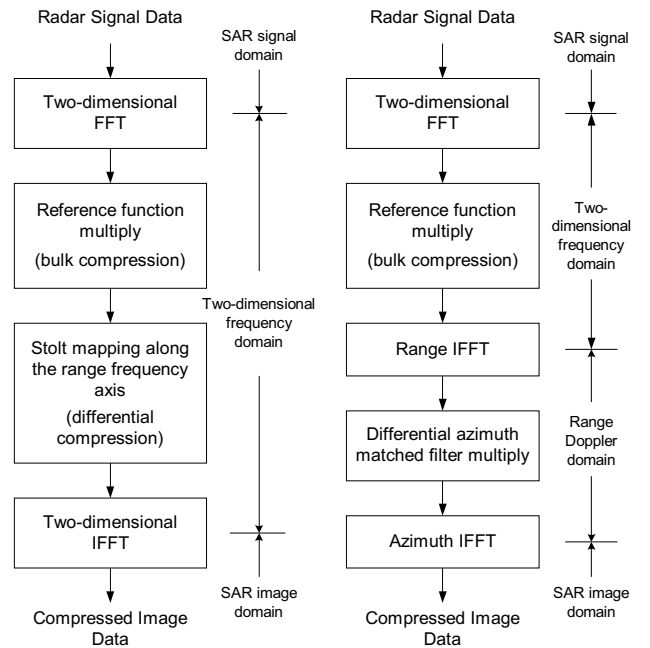


Figure 1: Block diagram of the ω KA

The accurate form of the algorithm consists of the following major steps:

1. FFTs are performed to transform the SAR signal data into the 2-D frequency domain. Assuming a hyperbolic form of the range equation, the resulting phase from a point target is

$$\theta_{2Df}(f_\tau, f_\eta) = -\frac{4\pi R_0}{c} \sqrt{(f_0 + f_\tau)^2 - \frac{c^2 f_\eta^2}{4V_r^2}} - \frac{\pi f_\tau^2}{K_r} \quad (1)$$

where f_τ and f_η are the range and azimuth frequencies, R_0 is the range of closest approach, f_0 is the radar center frequency and K_r is the FM rate

of the linear chirp signal. V_r is the effective radar velocity and c is the speed of light. The phase (1) includes the target phase due to the range encoding, range cell migration (RCM), range-azimuth coupling, and azimuth encoding.

2. The first focusing step is a reference function multiply (RFM). The reference function is computed for a selected range, R_{ref} . A target at the reference range is correctly focused by the RFM, but targets away from that range are only partially focused. For this reason, the RFM can be considered as a ‘‘bulk compression’’.

After the RFM filtering, the phase remaining in the two-dimensional signal spectrum is approximately

$$\theta_{\text{RFM}}(f_\tau, f_\eta) \approx -\frac{4\pi(R_0 - R_{\text{ref}})}{c} \sqrt{(f_0 + f_\tau)^2 - \frac{c^2 f_\eta^2}{4V_r^2}} \quad (2)$$

3. The second focusing step is the Stolt mapping or interpolation [1]. It completes the focusing of targets away from the reference range by re-mapping the range frequency axis according to

$$\sqrt{(f_0 + f_\tau)^2 - \frac{c^2 f_\eta^2}{4V_r^2}} = f_0 + f'_\tau \quad (3)$$

To understand the Stolt mapping, the square root term on the LHS of (3) can be expanded to get

$$\sqrt{(f_0 + f_\tau)^2 - \frac{c^2 f_\eta^2}{4V_r^2}} \approx (f_0 + f_\tau) - \frac{c^2 f_\eta^2}{8V_r^2 (f_0 + f_\tau)^2} \quad (4)$$

plus higher order terms. If only the $(f_0 + f_\tau)$ term existed on the RHS of (4), an inverse range DFT would give perfect range compression and registration, as the IDFT of a sine wave is a sinc function and the frequency (i.e. registration) would not depend on f_η . But the extra terms in (4) represent residual misfocusing.

To achieve perfect range compression and registration, the mapping (3) transforms the original range frequency variable f_τ into the new range frequency variable f'_τ . In this way, the phase is now *linear* in the new range frequency variable f'_τ

$$\theta_{\text{Stolt}}(f'_\tau, f_\eta) = -\frac{4\pi(R_0 - R_{\text{ref}})}{c} (f_0 + f'_\tau) \quad (5)$$

and the range IDFT will result in perfect range compression and registration. The mapping has effectively removed all the phase terms higher than linear term, which also implements the residual azimuth phase and range-azimuth coupling. For this reason, the Stolt mapping can be viewed as ‘‘differential compression’’.

Note that the higher order phase terms of (4) have not been ignored, some of which are discarded in the CSA and RDA. For this reason, the ω KA is accurate even when the SAR aperture is very wide or the squint angle is large, as long as the hyperbolic range equation is accurate.

4. Finally a two-dimensional IDFT is performed to transform the data back to the time domain, i.e. the SAR image domain.

3 Interpretations of the Mapping

Several interpretations of the Stolt mapping exist for seismic processing [2]. In this section, an alternative interpretation is given, taken from a signal processing viewpoint. It uses the Fourier transform shift/modulation property, and helps explain how the mapping of the range frequency axis (3) performs the remaining focusing operations.

The phase (2) that remains after the RFM represents the residual RCM, azimuth modulation and range-azimuth coupling. These terms are mixed in the square root term, and are corrected simultaneously by the Stolt mapping. In order to understand how all these corrections can be done in one step, consider the expanded form of the phase after RFM

$$\theta_{\text{RFM}}(f_\tau, f_\eta) \approx -\frac{4\pi(R_0 - R_{\text{ref}})}{c} \dots \left[f_0 D(f_\eta) + \frac{f_\tau}{D(f_\eta)} - \frac{f_\tau^2}{2f_0 D^3(f_\eta)} - \frac{c^2 f_\eta^2}{4V_r^2 f_0} \right] \quad (6)$$

where terms up to quadratic in f_τ and f_η are kept. The quantity $D(f_\eta)$ is the range migration parameter

$$D(f_\eta) = \sqrt{1 - \frac{c^2 f_\eta^2}{4V_r^2 f_0^2}} \quad (7)$$

To simplify the discussion, the residual range-azimuth coupling can be ignored, leaving the dominant terms of residual azimuth modulation and residual RCM

$$\theta_{\text{RFM}}(f_\tau, f_\eta) \approx -2\pi \Delta\tau \left\{ f_0 D(f_\eta) + \frac{f_\tau}{D(f_\eta)} \right\} \quad (8)$$

where $\Delta\tau = 2(R_0 - R_{\text{ref}})/c$ is the range ‘‘time’’ measured from the reference range.

These two largest terms illustrate two distinct features of the Stolt mapping, the scaling and shifting. After the RFM, the phase is linear in the range frequency direction, but the ‘‘frequency’’ of the waveform varies with azimuth frequency. This is illustrated in Figure 2, where Panel (a) shows the real part of the point target signal (showing the phase contours of (8)), and the horizontal slices in

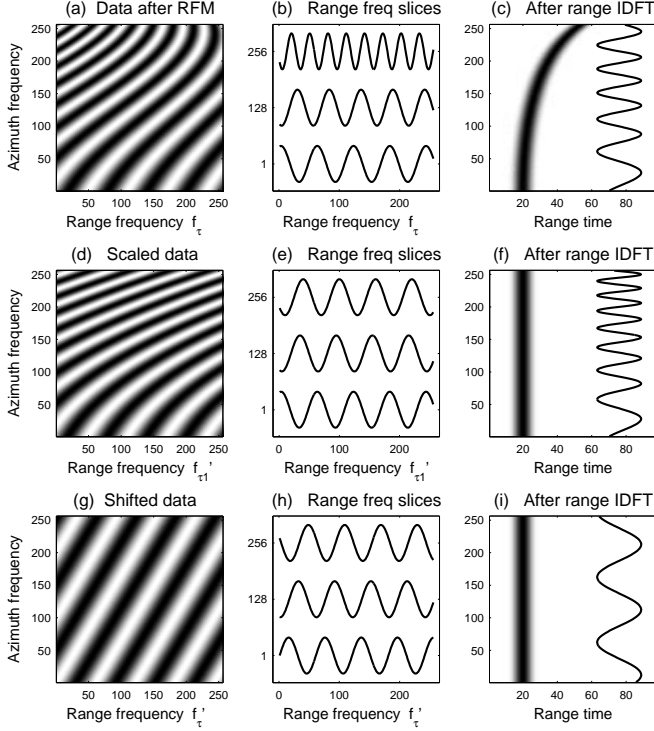


Figure 2: Interpretation of the scaling (row 2) and shifting (row 3) operations within the Stolt mapping

Panel (b) show how the waveform is a sine wave but with a “frequency” varying with azimuth frequency.

The frequency observed in the horizontal slices of Panel (b) represents the range position of the target, which becomes evident when the range IDFT is taken. This is shown in the thick line in Panel (c), where the residual RCM can be seen. Also, a quadratic phase is observed in the azimuth direction, as shown in the vertical slice (the thin line in Panel (c)). The quadratic phase represents azimuth modulation due to residual RCM and azimuth focusing.

In order to help understand Stolt mapping, it is broken down into two steps, corresponding to differential RCMC and azimuth compression.

3.1 Interpreting Differential RCMC

The residual RCM is represented by the second term of (8). The “frequency” of the waveform along the range frequency axis depends on f_η , as seen by the approximation

$$\frac{f_\tau}{D(f_\eta)} \approx f_\tau \left(1 + \frac{c^2 f_\eta^2}{8 V_r^2 f_0^2} \right) \quad (9)$$

If the range frequency axis is re-mapped so that $f_\tau/D(f_\eta)$ is replaced by f'_{τ_1} , the resultant phase becomes

$$\theta_{\text{RFM},1}(f'_{\tau_1}, f_\eta) = -2\pi \Delta\tau [f'_{\tau_1} + f_0 D(f_\eta)] \quad (10)$$

This component of the Stolt mapping involves a *stretching* of the range frequency axis by the factor D . The resultant phase is shown in Panel (d), and the horizontal slices of Panel (e) show that the “frequency” of the waveform is now independent of f_η . Then the subsequent range IDFT registers the data to a constant range, as shown in Panel (f), thereby accomplishing differential RCMC. But the azimuth modulation is still present, as seen in the thin line of Panel (f).

3.2 Interpreting Azimuth Compression

To consider the residual azimuth modulation, note that the mapping component of first term in (8) represents a *shift* of the range frequency variable by the amount

$$f_{\tau_{\text{shift}}} = f_0 [D(f_\eta) - 1] \approx -\frac{c^2 f_\eta^2}{8 V_r^2 f_0} \quad (11)$$

The phase resulting from this range frequency shift is shown in Panel (g). The shift removes the quadratic component of Panel (f), resulting in a phase that is now linear in both range frequency and azimuth frequency. This means that the residual azimuth compression has been done by this component of the Stolt mapping.

Replacing the terms of (8) by

$$f_0 + f'_\tau = f_0 D(f_\eta) + \frac{f_\tau}{D(f_\eta)} \quad (12)$$

and combining (9) and (11), we see that the Stolt mapping of the frequency variable f'_τ consists primarily of a scaling and a shifting

$$f'_\tau = f'_{\tau_1} + f_{\tau_{\text{shift}}} \quad (13)$$

which implements the differential RCMC and azimuth compression simultaneously. Although not involved in this interpretation, the residual range-azimuth coupling is also corrected by the accurate form of the mapping (3).

4 Approximate Form of the ω KA

Although the Stolt mapping looks simple mathematically, each sample in (f'_τ, f_η) space has to be individually interpolated to obtain the modified 2-D frequency domain signal. This is a time consuming step, but the approximate form of the ω KA shown in Figure 1 offers a simpler solution.

After RFM step, there are three main phase components (6), and the dominant one is the residual azimuth modulation. In the approximate version of ω KA, the smaller differential RCMC and SRC components are ignored [3, 4, 5]. This means that the differential azimuth compression can be implemented by a simple shift of the range frequency axis, as described in Section 3.2. This is

easier, as the shift can be implemented simply by a phase rotation in the range Doppler domain.

This approximation means that the residual RCM and range-azimuth coupling are assumed to be independent of range, a feasible assumption if the SAR aperture is not too wide and the squint is low. To see if the approximation is sufficiently accurate, the phase error in the approximation

$$\sqrt{(f_0 + f_\tau)^2 - \frac{c^2 f_\eta^2}{4V_r^2}} \approx (f_0 + f_\tau) - \frac{c^2 f_\eta^2}{8V_r^2 f_0^2} \quad (14)$$

can be examined for the radar parameters under consideration. Equation (14) is obtained by modifying (4) according to the azimuth compression shift (11).

Comparison with the RDA and CSA

Some comparisons of the ω KA with other processing algorithms can be found in [4, 6]. Here are some further thoughts:

RDA: In the accurate version of the RDA, SRC is applied with an azimuth frequency dependence, but without a range dependence. The approximate version of the ω KA applies SRC with the same dependencies, because SRC is only applied in the 2-D frequency domain with the RFM. However, the RDA is often used in its less accurate form where SRC is not varied with range or azimuth frequency.

In terms of RCMC, the RDA uses a range dependent RCMC, while the approximate ω KA uses a range invariant RCMC. Also, it is interesting to note that V_r can be allowed to vary with range in the RDA and in the *approximate* version of the ω KA, but not in the “accurate” ω KA.

CSA: In the CSA, the chirp scaling operation performs differential RCMC, but not differential SRC, and its residual azimuth compression allows V_r to vary. In this sense, its accuracy lies between the accurate and approximate versions of the ω KA. In fact, the approximate version of the ω KA is equivalent to the CSA without the chirp scaling operation.

5 Discussion of Errors

The use of a constant V_r in the ω KA introduces errors in RCMC, SRC and azimuth matched filtering. The dominant error comes from the linear RCM. For an exposure time of T_a , a squint angle of θ_{sq} , and a velocity error of ΔV_r , the linear migration error is

$$\Delta \text{RCM}_{\text{linear}} = \Delta V_r \sin \theta_{sq} T_a \quad (15)$$

The constant V_r approximation is valid for airborne but not for satellite cases. For a typical C-band satellite SAR,

where V_r varies by 0.5% over 100 km, the residual RCM is less than 1 m. This is small compared to the processed resolutions. However, the error is 4 times larger for L-band satellites, and can become significant when the swaths are wider and the resolution is finer, so these cases should be evaluated individually.

The *approximate* version of the ω KA assumes a range invariant RCMC and SRC [4], and once again the residual RCM is the dominant error. Its maximum value is several meters for typical SARs, satellite or airborne. This error is likely allowable for current satellite SARs, but probably not for airborne SARs that have finer resolutions.

6 Conclusions

We have discussed two versions of the ω KA, and compared them to the CSA and RDA. Unlike the RDA and CSA, the differential focusing of the ω KA is done in the two dimensional frequency domain, using an interpolation operation. This is an unusual operation in the signal processing field, and requires some explanation.

The differential focusing corrects for the range variation of RCM, range/azimuth coupling and the azimuth FM rate in the SAR signal. By examining each component separately, we show how the range frequency interpolation or mapping corrects each of the range-variant parts of the focusing.

The ω KA proves to be very accurate for most wide-aperture, high-squint situations. However, some approximations have to be made, notably the constant velocity assumption, which makes their error properties different from the RDA and CSA. This affects which SAR processing algorithm should be chosen for each imaging case.

References

- [1] R. H. Stolt. Migration by Transform. *Geophysics*, 43(1): pp. 23–48, February 1978.
- [2] J. H. Chun and C. A. Jacowitz. Fundamentals of Frequency Domain Migration. *Geophysics*, 46: pp. 717–733, 1981.
- [3] C. Cafforio, C. Prati, and F. Rocca. SAR Data Focusing Using Seismic Migration Techniques. *IEEE Trans. on Aerospace and Electronic Systems*, 27(2): pp. 194–207, March 1991.
- [4] R. Bamler. A Comparison of Range-Doppler and Wave-number Domain SAR Focussing Algorithms. *IEEE Trans. Geosc. and Rem. Sens.*, 30(4):706–713, July 1992.
- [5] W. G. Carrara, R. S. Goodman, and R. M. Majewski. *Spotlight Synthetic Aperture Radar Signal Processing Algorithms*. Artech House, Norwood, MA, 1995.
- [6] T. E. Scheuer and F. H. Wong. Comparison of SAR Processors Based on a Wave Equation Formulation. In *Proc. Int. Geoscience and Remote Sensing Symp., IGARSS'91*, volume 2, pages 635–639, Finland, June 1991.